Theoretical study of magnetic domain walls through a cobalt nanocontact

László Balogh, Krisztián Palotás, László Udvardi and László Szunyogh

Department of Theoretical Physics
Budapest University of Technology and Economics

Budapest, 22 June 2012

This work has been developed in the framework of the project "Talent care and cultivation in the scientific workshops of BME" project. This project is supported by the grant **TÁMOP-4.2.2.B-10/1–2010-0009**

Table of contents

The Kondo effect in ferromagnetic atomic contacts

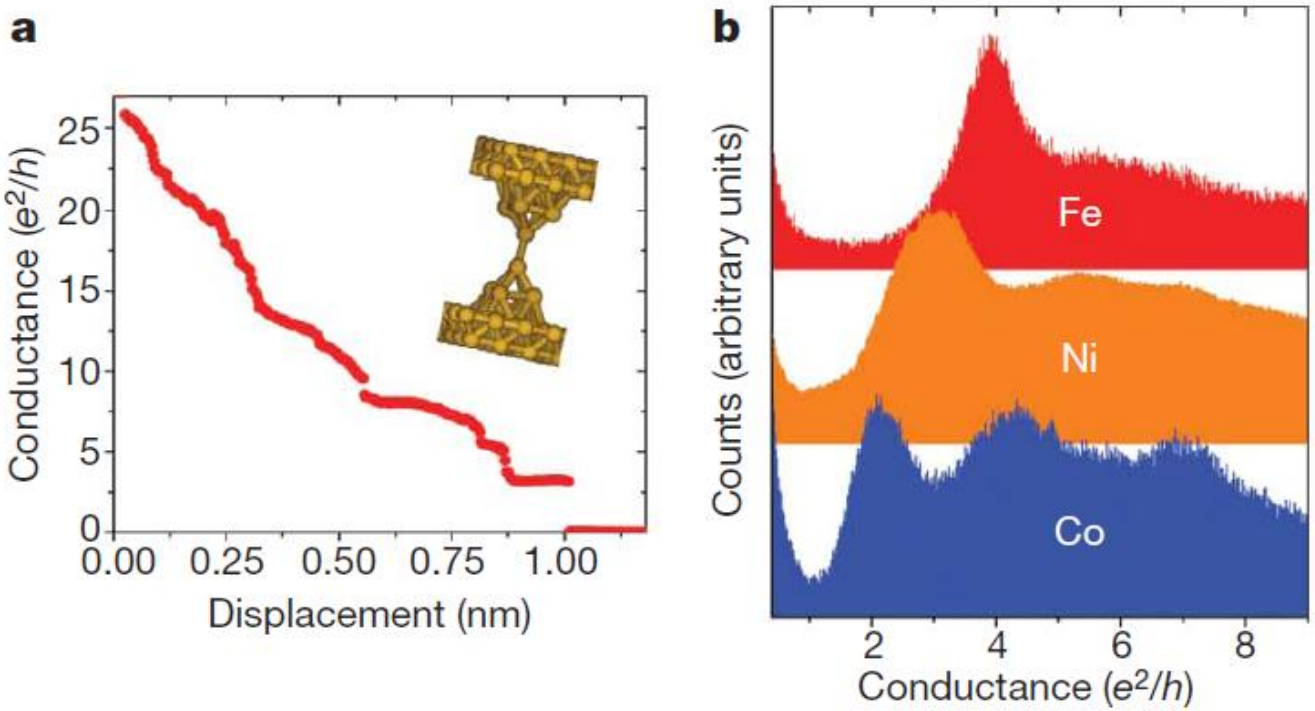

Figure 1 | Conductance of a monatomic contact. a, Example of a trace where we record the conductance while stretching a nickel wire using a scanning tunnelling microscope (STM) at 4.2 K. Inset, model of a monatomic contact. **b**, Conductance histograms constructed for iron, cobalt and nickel from thousands of such traces. The position of the first peak of in each histogram corresponds to the conductance of the monatomic contact. **c**, Differential

M. R. Calvo, *et al.*, Nature, **458,** 1150, (2009)

The Kondo effect in ferromagnetic atomic contacts

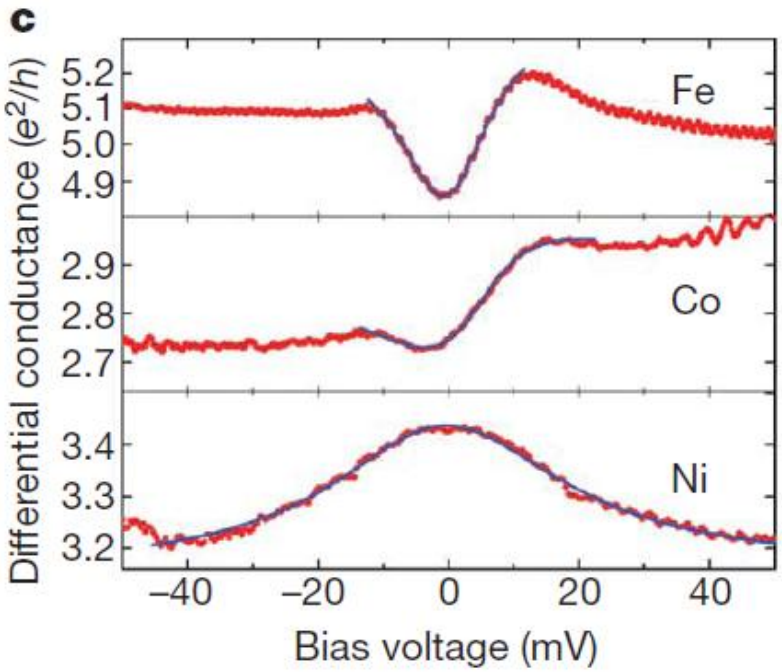

$$\frac{\mathrm{d}I}{\mathrm{d}V} = g_0 + \frac{A}{1+q^2}\frac{(q+\varepsilon)^2}{1+\varepsilon^2}$$

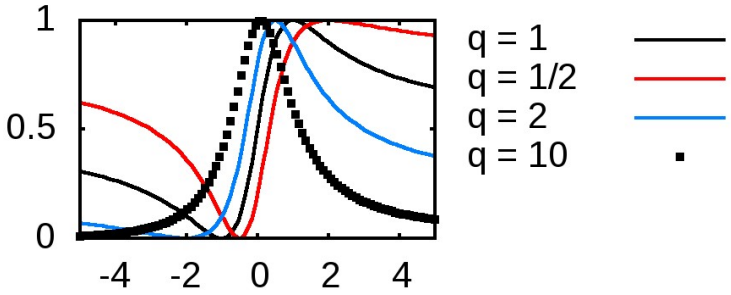

c, Differential conductance curves recorded at the monatomic contact as a function of the applied voltage. A characteristic resonance appears at small bias that fits the Fano line shape. All possible symmetries are found in the spectroscopy of iron, cobalt and nickel contacts, and the width of the resonance is the main difference between the spectra of the three materials. This width is proportional to the Kondo temperature.

M. R. Calvo, *et al.*, Nature, **458,** 1150, (2009)

The Kondo effect in ferromagnetic atomic contacts

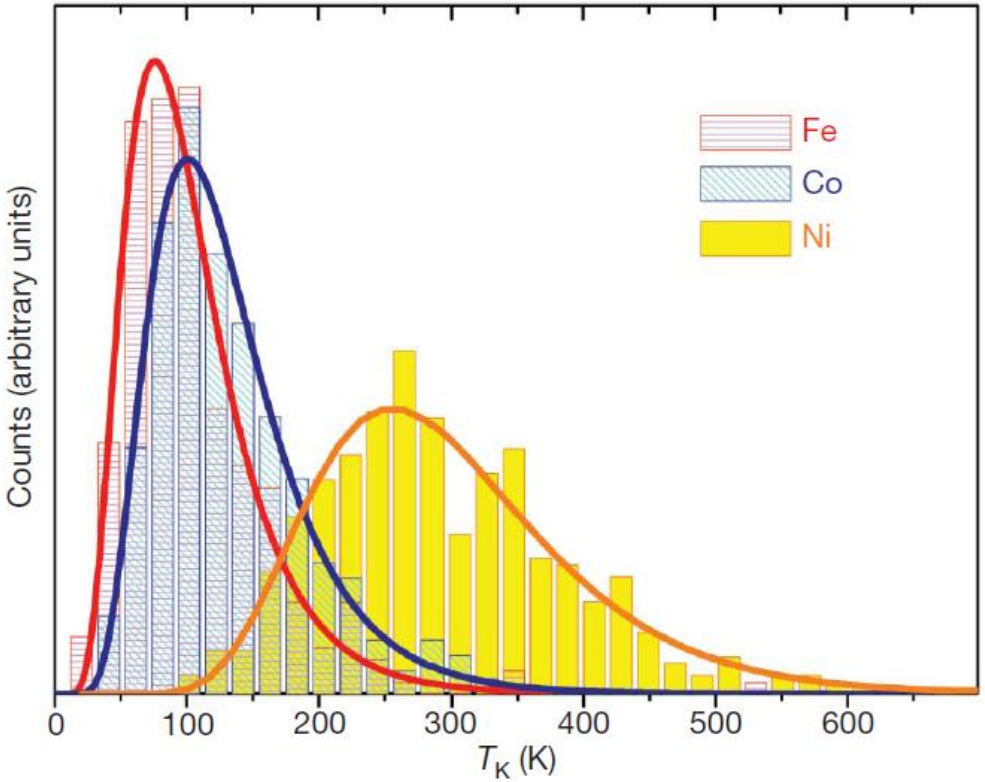

Figure 2 | Histograms of inferred Kondo temperatures for iron, cobalt and nickel. The histograms are constructed from more than 200 fittings and normalized to the total number of curves fitted. The continuous lines show the fits of the data to log-normal distributions of T_K with a different most probable value for each material.

M. R. Calvo, *et al.*, Nature, **458,** 1150, (2009)

Model of the nanocontact

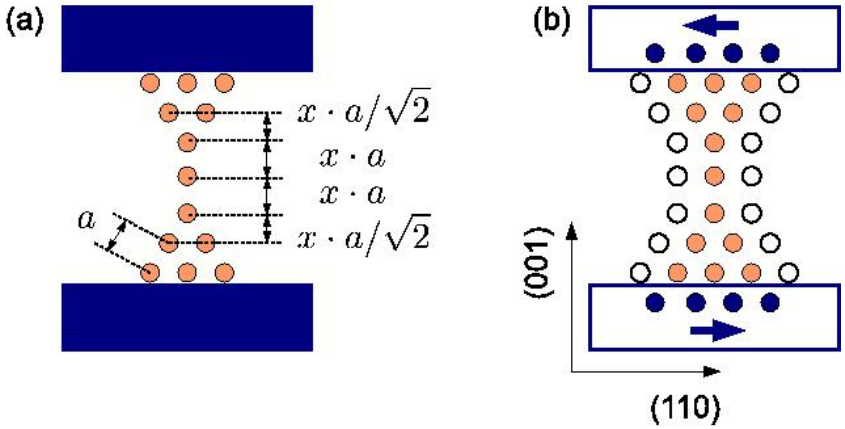

Model of the nanocontact

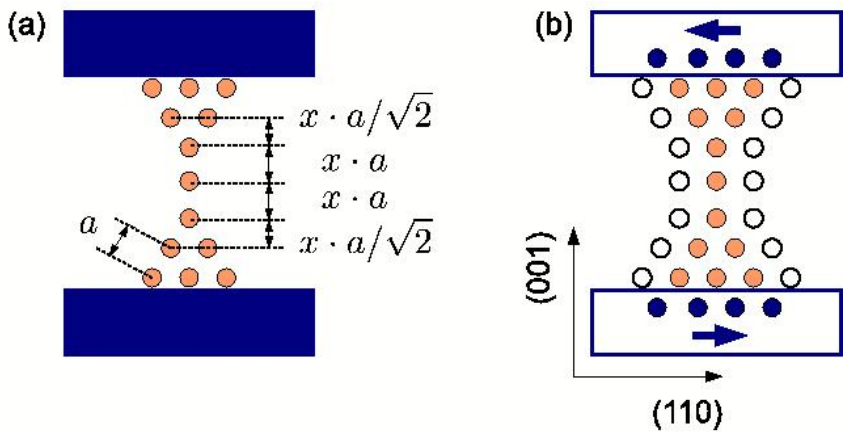

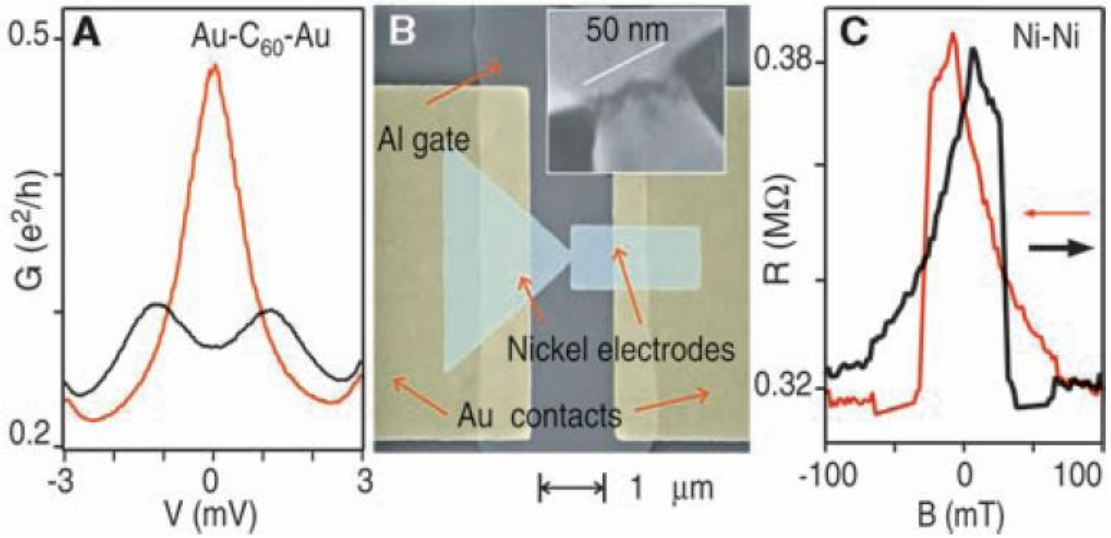

Fig. 1. (**A**) Kondo signal for C_{60} with Au electrodes at $T = 1.5$ K. At $B = 0$ (red line), there is a zero-bias peak in $G(V)$ that becomes split for $B = 10$ T (black line). (**B**) Scanning electron micrograph of a Ni break junction. The magnetic field is applied in the horizontal direction. (**Inset**) Close-up of the junction region after electromigration. (**C**) Tunneling magnetoresistance near $V = 0$ at $T = 4.2$ K of a Ni contact after electromigration, with no C_{60} molecule present.

A. N. Pasupathy, *et al.*, Science, **306,** 86, (2004)

Heisenberg model I.

- $\mathcal{H} = \frac{1}{2}\sum_{ij} J_{ij}\vec{\sigma}_i\vec{\sigma}_j$: invariant under global spin rotation
- Boundary condition: invariant under global spin rotation around the (110) direction

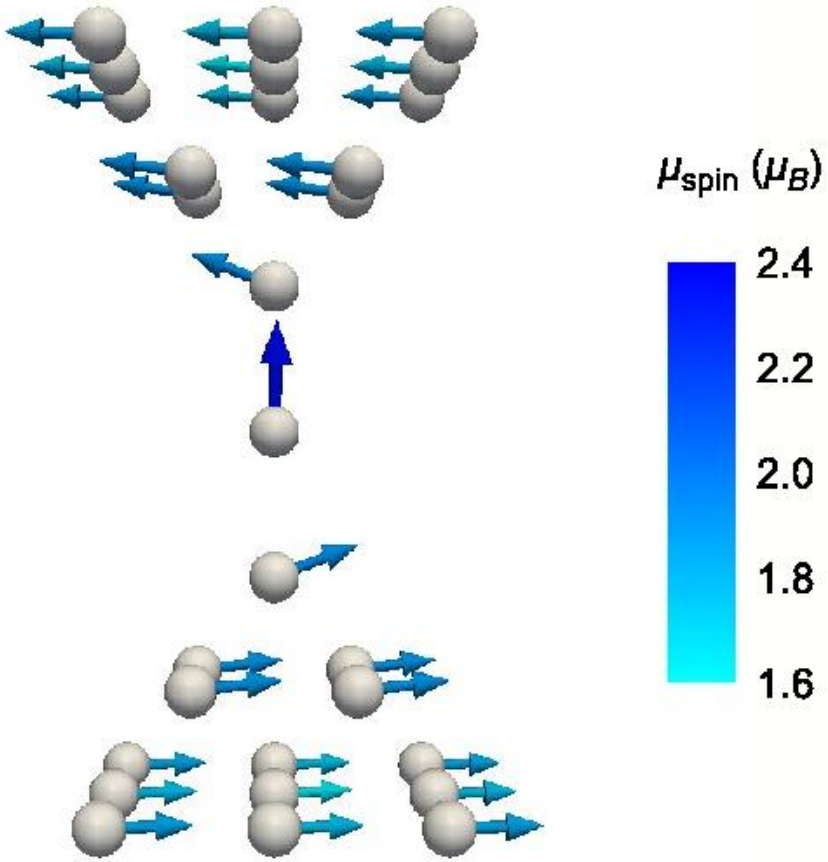

Heisenberg model I.

- $\mathcal{H} = \frac{1}{2}\sum_{ij} J_{ij}\vec{\sigma}_i\vec{\sigma}_j$: invariant under global spin rotation
- Boundary condition: invariant under global spin rotation around the (110) direction

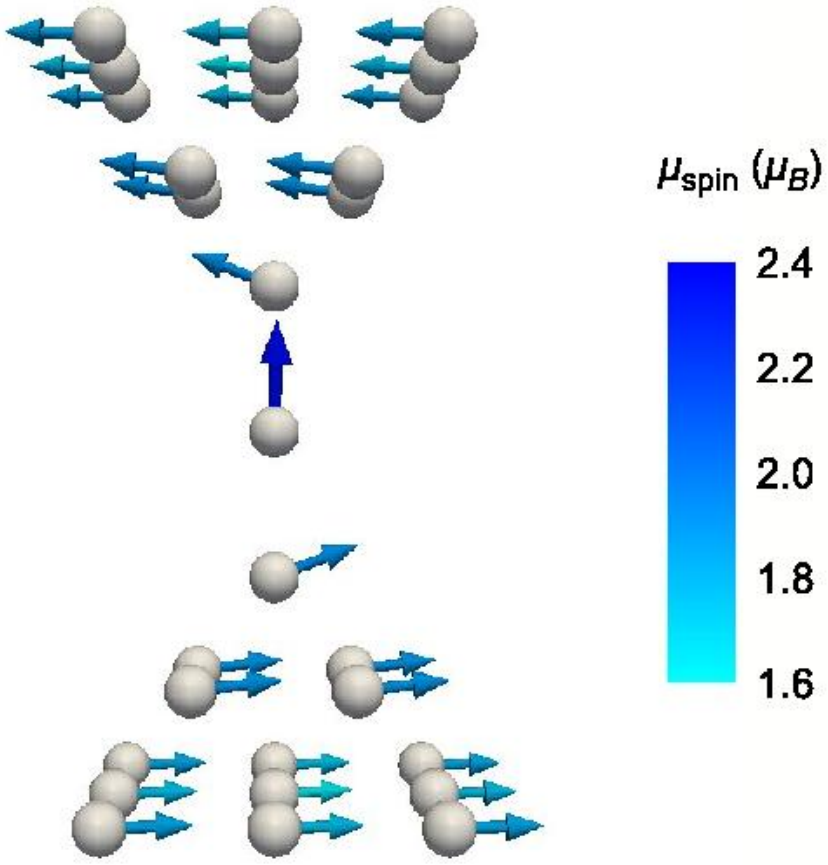

Heisenberg model II.

- Higher order terms

$$\mathcal{H}_{\square} = J_{\square}\left[\,(\vec{\sigma}_1\vec{\sigma}_2)\,(\vec{\sigma}_3\vec{\sigma}_4) + (\vec{\sigma}_2\vec{\sigma}_3)\,(\vec{\sigma}_4\vec{\sigma}_1) + (\vec{\sigma}_1\vec{\sigma}_3)\,(\vec{\sigma}_2\vec{\sigma}_4)\,\right]$$

(see, e.g., S. Lounis, P. H. Dederichs, Phys. Rev. B **82,** 180404 (2009))

- Tensorial couplings (SOC)

$$\begin{aligned}\mathcal{H} = &\left(\frac{1}{3}\mathrm{Tr}\,\mathbf{J}_{ij}\right)\mathbf{I}\\ &+\frac{1}{2}\left(\mathbf{J}_{ij}+\mathbf{J}_{ij}^{T}\right)-\mathbf{J}_{ij}^{\mathrm{I}}\\ &+\frac{1}{2}\left(\mathbf{J}_{ij}-\mathbf{J}_{ij}^{T}\right)\end{aligned}$$

- On-site anisotropy (SOC)

$$K(\theta) = -K_2\sin^2(\theta)$$

Rotational energy

We rotated the exchange field at each atomic sites around the (110) axis.

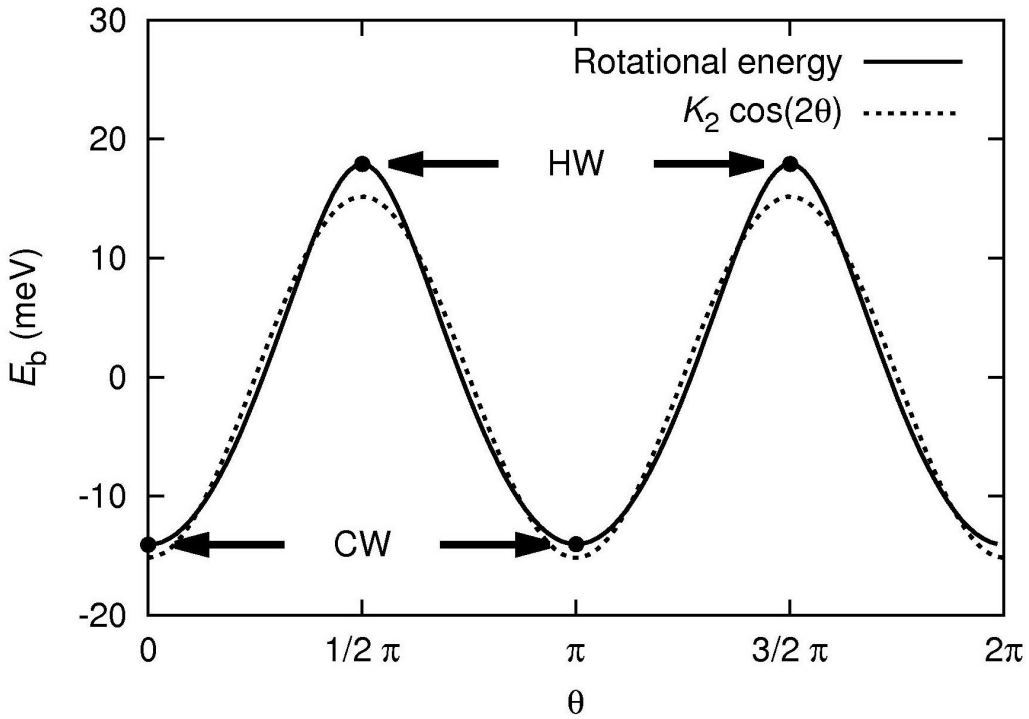

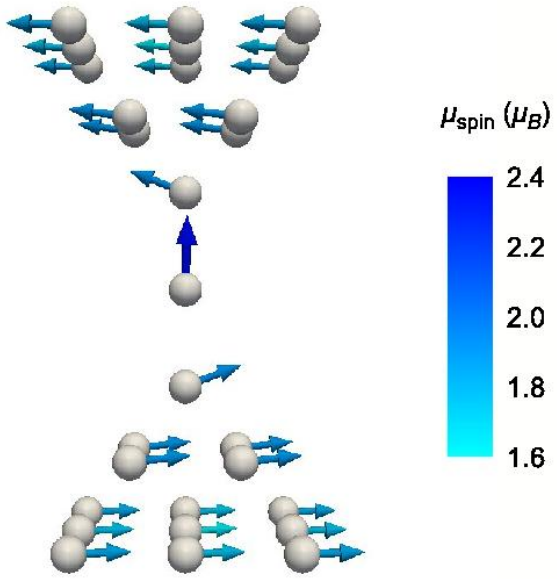

Dashed line: $-15.2\,[\mathrm{meV}]\,\cos(2\theta)$

Helical Wall

Cycloidal Wall

Calculation I.: KKR

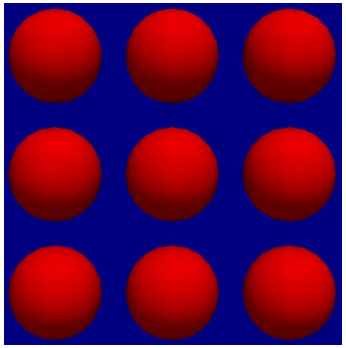

- Potential = atomic potentials + constant
- *Scattering path operator:*

$$\boldsymbol{\tau}(\varepsilon) = \left(\mathbf{t}(\varepsilon)^{-1} - \mathbf{G}_0(\varepsilon)\right)^{-1}$$

- Band energy: $E_\mathrm{b} = -\frac{1}{\pi}\mathrm{Im}\int_{-\infty}^{\varepsilon_\mathrm{F}} \mathrm{Tr}\ln\boldsymbol{\tau}(\varepsilon)\,\mathrm{d}\varepsilon$

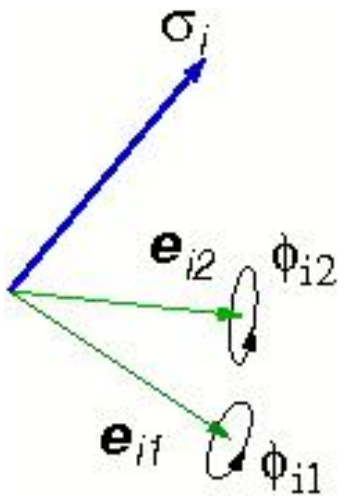

- Change of the single site t-matrix:

$$\Delta t_i = i[\mathbf{e}_{i\alpha}\mathbf{J}, t_i]\Delta\phi_{i\alpha}$$

- First derivative of the band energy:

$$\frac{\partial E_\mathrm{b}}{\partial\phi_{i\alpha}} = \frac{1}{\pi}\mathrm{Re}\int_{-\infty}^{\varepsilon_\mathrm{F}} \mathrm{Tr}\left\{\tau_{ii}\left[\mathbf{e}_{i\alpha}\mathbf{J}, m_i\right]\right\}\,\mathrm{d}\varepsilon$$

Calculation II.: Newton-Raphson

- Derivatives of E_b: $\dfrac{\partial E_\mathrm{b}}{\partial \phi_{i\alpha}} = \dots \qquad \dfrac{\partial^2 E_\mathrm{b}}{\partial \phi_{i\alpha} \partial \phi_{j\beta}} = \dots$
- Newton-Raphson iteration: $x_{n+1} = x_n - \dfrac{f'(x_n)}{f''(x_n)}$

- Starting configuration: MC simulated annealing
- Once the Newton-Raphson iteration has converged,
- new effective potentials are generated
- and the procedure is repeated until the effective potential converged and the "gradient" E_b is disappeared.

Uniaxial anisotropy

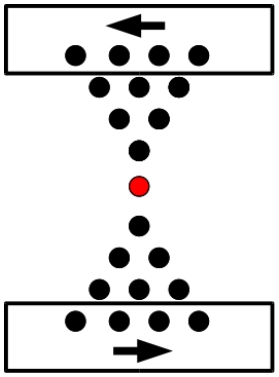

$$E_{\text{band}}(\underbrace{\ldots}_{\text{fixed}}, \vartheta, \varphi, \underbrace{\ldots}_{\text{fixed}}) =$$

$$\sum_{\ell=0}^{\infty} \sum_{m=-\ell}^{\ell} K_\ell^m Y_\ell^m(\vartheta, \varphi)$$

Uniaxial anisotropy:

$$K_2^0 \cdot \frac{1}{4}\sqrt{\frac{5}{\pi}}\,(3z^2 - 1)$$

Uniaxial anisotropy

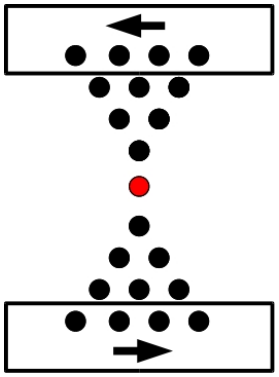

$$E_{\text{band}}(\underbrace{\ldots}_{\text{fixed}}, \vartheta, \varphi, \underbrace{\ldots}_{\text{fixed}}) =$$

$$\sum_{\ell=0}^{\infty} \sum_{m=-\ell}^{\ell} K_\ell^m Y_\ell^m(\vartheta, \varphi)$$

Uniaxial anisotropy:

$$K_2^0 \cdot \frac{1}{4}\sqrt{\frac{5}{\pi}}\,(3z^2 - 1)$$

	$E_{\text{HW}} - E_{\text{CW}}$	$\frac{3}{4}\sqrt{\frac{5}{\pi}}K_2^0$
85%	13.4	24.0
90%	20.5	28.4
95%	28.1	31.4
100%	32.0	30.6
105%	32.1	29.2
110%	30.5	26.9
115%	27.8	24.2

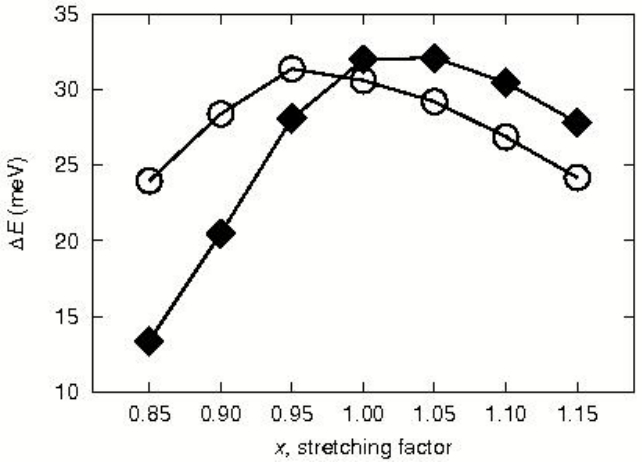

Decreased coordination = increased moments and anisotropy

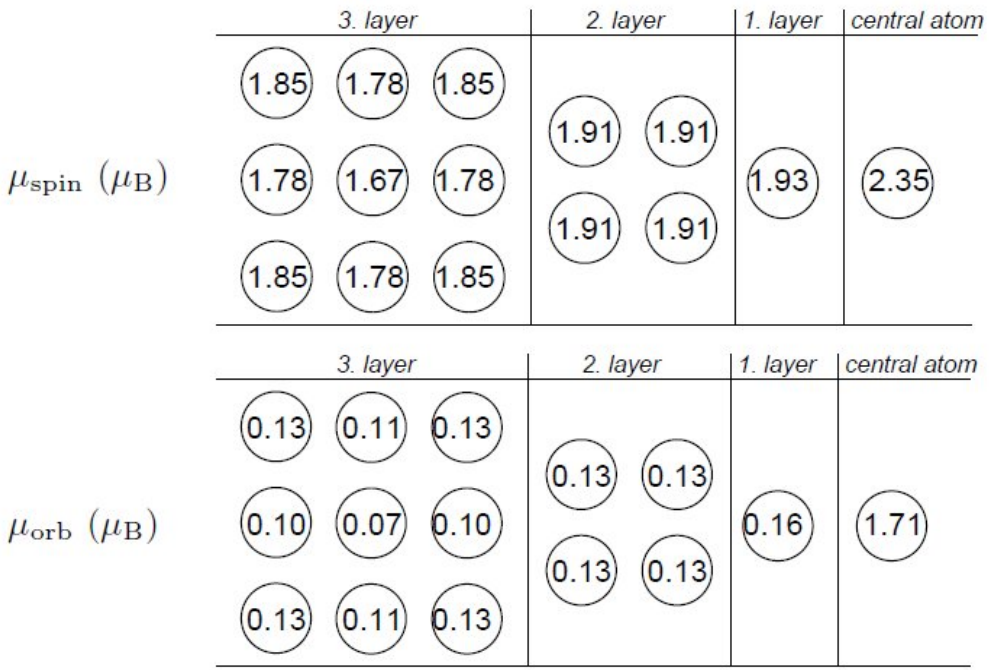

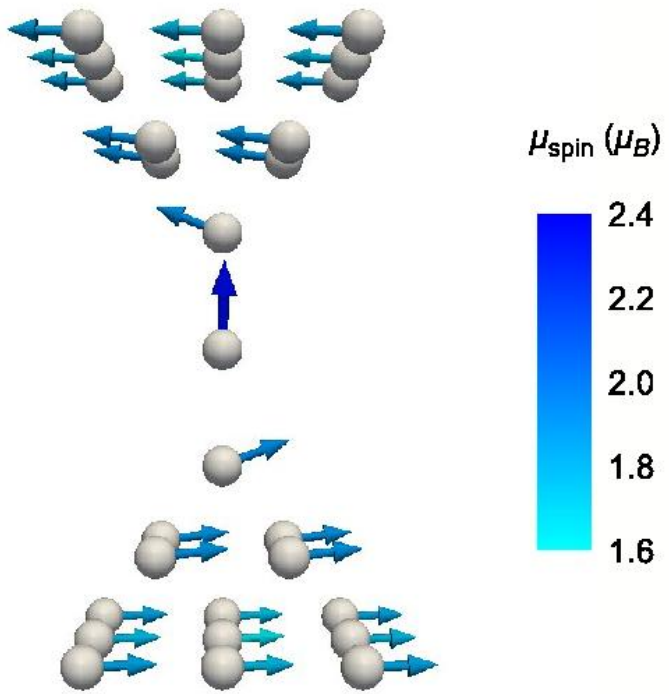

- Top layer: $\mu_{\rm spin} = 1.82\,\mu_{\rm B}$; $\mu_{\rm orb} = 0.14\,\mu_{\rm B}$
- Bulk: $\mu_{\rm spin} = 1.67\,\mu_{\rm B}$; $\mu_{\rm orb} = 0.08\,\mu_{\rm B}$

Expansion coefficients K_ℓ^m (meV)

Table II. Expansion coefficients K_ℓ^m (in units of meV) of the band energy of the contact, see Eq. (9), according to real spherical harmonics R_ℓ^m up to $\ell = 4$.

ℓ	m	R_ℓ^m	$x = 0.85$	$x = 0.90$	$x = 0.95$	$x = 1.00$	$x = 1.05$	$x = 1.10$	$x = 1.15$
1	0	$\frac{1}{2}\sqrt{\frac{3}{\pi}}z$	−240	−247	−235	−212	−192	−176	−159
2	0	$\frac{1}{4}\sqrt{\frac{5}{\pi}}\left(3z^2-1\right)$	−25.3	−30.0	−33.2	−32.4	−30.9	−28.4	−25.6
2	2	$\frac{1}{4}\sqrt{\frac{15}{\pi}}\left(x^2-y^2\right)$	4.30	2.54	1.39	0.51	−0.29	−0.92	−1.36
3	0	$\frac{1}{4}\sqrt{\frac{7}{\pi}}\left(5z^3-3z\right)$	4.12	3.06	1.63	0.71	−0.28	−1.43	−2.67
3	2	$\frac{1}{4}\sqrt{\frac{105}{\pi}}\left(x^2-y^2\right)z$	−0.199	−0.093	0.004	0.108	0.196	0.267	0.293
4	0	$\frac{3}{16}\sqrt{\frac{1}{\pi}}\left(35z^4-30z^2+3\right)$	−0.63	1.72	4.60	4.94	5.05	4.85	4.32
4	2	$\frac{3}{8}\sqrt{\frac{5}{\pi}}\left(x^2-y^2\right)\left(7z^2-1\right)$	0.033	0.125	0.184	0.108	0.051	0.001	−0.052
4	4	$\frac{3}{16}\sqrt{\frac{35}{\pi}}\left(x^4-6x^2y^2+y^4\right)$	−0.007	−0.005	−0.018	−0.041	−0.088	−0.187	−0.345

$$E(\vec{\sigma}) = E_{\text{anis}}(\vec{\sigma}) + \vec{\sigma}\sum_j \mathbf{J}_{\text{c}j}\vec{\sigma}_j$$

The D_{4h} point-group allows the following terms:

$$E_{\text{anis}}(\vec{\sigma}) = K_2^0 R_2^0(\vec{\sigma}) + K_4^0 R_4^0(\vec{\sigma}) + K_4^4 R_4^4(\vec{\sigma})$$

Summary

Manuscript

http://arxiv.org/abs/1205.4579

Summary

- We have developed a computational technique on *first principle* footing to find non-collinear ground state of complex magnetic clusters.
- The formation of the cycloidal wall against a helical wall is primarily driven by the uniaxial on-site anisotropy at the cetral site.

Summary

Manuscript

http://arxiv.org/abs/1205.4579

Summary

- We have developed a computational technique on *first principle* footing to find non-collinear ground state of complex magnetic clusters.
- The formation of the cycloidal wall against a helical wall is primarily driven by the uniaxial on-site anisotropy at the cetral site.

The End.

Thank you for your attention